ESTIMATION OF VIBRATIONAL POWER IN BUILT-UP SYSTEMS INVOLVING BOX-LIKE STRUCTURES, PART 1: UNIFORM FORCE DISTRIBUTION

R. A. FULFORD[†] AND B. A. T. PETERSSON

AAETS, Loughborough University, Loughborough LE11 3TU, England

For the vibration analysis of built-up structures traditional point-like connections cannot be applied where the interface is large and the wavelength is small. In these situations the spatially distributed wavefield has to be accounted for, whereby the field properties associated with the interface (i.e., velocity, force) have to be considered to be continuous over a surface or, for a one-dimensional contact, along a line. Due to the perceived complexity of these distributions it is most common for analyses to employ a numerical technique which, whilst efficient as a methodology, is limited in that little is revealed about the physics of the system. The solutions can therefore be rather esoteric and in conjunction with design this makes the techniques cumbersome to use. As a move towards overcoming the problem the work presented considers a simplified analytical approach from which a model of a box-like structure is obtained. The basis of the approach is to consider the spatial properties of distributed forces in terms of their Fourier components and then hypothesize that the zero order, i.e., the uniform component, is dominant. In this way, the true spatial characteristics of the forces are retained but in a reduced and elementary form. This greatly simplifies the modelling. For the box-like structure, supported by an infinite plate-like recipient, a prediction of the vibratory power is considered and qualifying results established.

© 2000 Academic Press

1. INTRODUCTION

In many installations, machinery is mounted upon supports which have a box-like structure and the wavenumber condition is such that the force and velocity fields are spatially distributed along the plate interfaces. In this situation each face of the box supports a wavefield and, with respect to an analysis of the dynamic response, neither point-like nor rigid-body simplifications are applicable. Without these simplifications, the analysis becomes extensive and the analyst resorts, most often, to computer-based numerical techniques. Whilst as a strength these techniques offer an efficient methodology, one inherent cost is that they reveal little about the physics of the system. Consequently, they offer only a limited understanding of the structural behaviour. The importance of this is that without physical insight the forthcoming solution is relevant only to the particular system being studied and cannot be immediately extended to aid the analysis of another, even related, system. Numerical techniques in conjunction with engineering design often necessitate, therefore, many repeated 'test' calculations and the work can become rather capricious. With this in mind the development of an analytical model through which an understanding of the structural behaviour can be accorded is considered most useful.

[†] Now at, Institut für Technische Akustik, Technische Universität Berlin, 10587 Berlin, Germany.

As a move towards this goal it is recognized that where a box consists of four side-walls and a top-plate, a sub-study can be resolved as the vibrational response of a single side-wall subjected to an arbitrary force distributed along its upper edge. Whilst in the context of a box structure it is possible for this force to excite both flexural and in-plane motion work by Fulford and Petersson [1] details that where the thicknesses of the side-wall and the top-plate differ by a factor of two, the dominating transmission path via the side-wall is governed by the in-plane components. Under this condition the arbitrary force excitation at the top edge can, with little compromise to the applicability of the model, be considered to have a translational component only.

Thence for a side-wall of width L in co-ordinate direction x, excited along its upper edge by a distributed, in-plane, translational force only, the total complex power is given [2] as

$$Q_{top} = \frac{1}{2} \left\{ \int_0^L \int_0^L Y(x|x_0) F(x_0) F^*(x) \, \mathrm{d}x \, \mathrm{d}x_0 \right\}, \tag{1}$$

where the active power input to the side-wall, W_{top}, is readily obtained by taking the real part. A list of symbols is given in Appendix B.

When both the real and imaginary components of the distributed force are considered to comprise a uniform component equal to their respective spatial averages together with a spatially varying, complex component such that

$$F(x) = f_{av}^{\Phi} \left[1 + \frac{f^{\Phi}(x)}{f_{av}^{\Phi}} \right] + \mathrm{i} f_{av}^{\Psi} \left[1 + \frac{f^{\Psi}(x)}{f_{av}^{\Psi}} \right], \tag{2}$$

an alternative form of equation (1) is obtained as

$$Q_{top} = \frac{1}{2} \int_0^L \int_0^L Y(x|x_0) \left\{ (f_{av}^{\Phi})^2 \left[1 + \frac{f^{\Phi}(x)}{f_{av}^{\Phi}} \right] \left[1 + \frac{f^{\Phi}(x_0)}{f_{av}^{\Phi}} \right] \right.$$

$$\left. + (f_{av}^{\Psi})^2 \left[1 + \frac{f^{\Psi}(x)}{f_{av}^{\Psi}} \right] \left[1 + \frac{f^{\Psi}(x_0)}{f_{av}^{\Psi}} \right] \right\} \mathrm{d}x \, \mathrm{d}x_0. \tag{3}$$

When $f^{\Phi}(x)$ and $f^{\Phi}(x)$ fluctuate, with x, about zero, their spatial integrals tend to be small in comparison with those associated with f_{av}^{Φ} and f_{av}^{Ψ}. Under these conditions, equation (1) reduces to

$$Q_{\omega\rho} = \frac{1}{2} |f_{av}|^2 \int_0^L \int_0^L Y(x|x_0) \, \mathrm{d}x \, \mathrm{d}x_0. \tag{4}$$

Accordingly it can be hypothesized that, for a practically interesting range of Helmholtz numbers, the distributed force has a dominant uniform component. Hence, a reliable estimate of the power would follow from substituting the uniform component for the "true" spatially varying force distribution. The reasoning leading to equation (4) implies, of course, that to test the hypothesis any physically conceivable force distribution is admissible.

The significance of the hypothesis is that it permits the spatial attributes of the force in the line integral to be encompassed using only a magnitude "scaling" component. In turn this greatly simplifies the mathematics so that equation (1) is reduced to equation (4). Moreover,

a uniform distribution in the spatial domain is equivalent to the nought component in the wavenumber domain such that, by the same argument, when the response of the side-wall is expressed as a summation of Fourier components a reliable estimate of the power is forthcoming using only the zeroth order term.

2. POWER TRANSMISSION FOR A SIDE-WALL

For in-plane motion the wavefield in any structure comprises both longitudinal and shear waves,

$$\nabla^2 \phi = \frac{1}{c_L^2} \frac{\partial^2 \phi}{\partial t^2}, \tag{5}$$

$$\nabla^2 \psi = \frac{1}{c_T^2} \frac{\partial^2 \psi}{\partial t^2}, \tag{6}$$

where ϕ represents the dilatational part of the field and ψ the rotational. The potential and shear functions [3] are defined as

$$\phi = \frac{\partial u}{\partial x} + \frac{\partial v}{\partial y}, \tag{7}$$

$$\psi = \frac{1}{2} \left(\frac{\partial v}{\partial x} - \frac{\partial u}{\partial y} \right), \tag{8}$$

respectively. The longitudinal and shear wave speeds, c_L, c_T are given by

$$c_L = \sqrt{E/\rho(1 - v^2)}, \tag{9}$$

$$c_T = \sqrt{G/\rho}, \tag{10}$$

when a thin plate is assumed so that the state of stress is plane.

If the side-wall is infinite in length, a solution in the wavenumber domain can be found by realizing that along both the upper and lower edges, the longitudinal and shear waves are coupled together through a common trace wavenumber k. Assuming harmonic motion, the solutions to equations (5) and (6) become

$$\phi(\omega, k) = (A_1 e^{ik_\phi y} + B_1 e^{-ik_\phi y}) e^{ikx + i\omega t}, \tag{11}$$

$$\psi(\omega, k) = (A_2 e^{ik_\psi y} + B_2 e^{-ik_\psi y}) e^{ikx + i\omega t}, \tag{12}$$

where

$$k_\phi^2 = k_L^2 - k^2, \tag{13}$$

$$k_\psi^2 = k_T^2 - k^2. \tag{14}$$

Application of equations (7) and (8), together with Hooke's law, yields expressions for the stresses in the plate,

$$\sigma_y(k) = \left\{ \left(D + 2G\frac{k_\phi^2}{k_L^2} \right) e^{ik_\phi y} A_1 + \left(D + 2G\frac{k_\phi^2}{k_L^2} \right) e^{-ik_\phi y} B_1 - \frac{4Gkk_\psi}{k_T^2} e^{ik_\psi y} A_2 \right.$$

$$\left. + \frac{4Gkk_\psi}{k_T^2} e^{-ik_\psi y} B_2 \right\} e^{ikx}, \tag{15}$$

$$\sigma_y(k) = \left\{ \left(D + 2G\frac{k^2}{k_L^2} \right) e^{ik_\phi y} A_1 + \left(D + 2G\frac{k^2}{k_L^2} \right) e^{-ik_\phi y} B_1 + \frac{4Gkk_\psi}{k_T^2} e^{ik_\psi y} A_2 \right.$$

$$\left. - \frac{4Gkk_\psi}{k_T^2} e^{-ik_\psi y} B_2 \right\} e^{ikx}, \tag{16}$$

$$\tau_w(k) = \left\{ \frac{-2Gkk_\phi e^{ik_\phi y}}{k_L^2} A_1 + \frac{2Gkk_\phi e^{-ik_\phi y}}{k_L^2} B_1 + \frac{2G(k^2 - k_\psi^2)e^{ik_\psi y}}{k_T^2} A_2 \right.$$

$$\left. + \frac{2G(k^2 - k_\psi^2)e^{-ik_\psi y}}{k_T^2} B_2 \right\} e^{ikx}, \tag{17}$$

where the time dependence has been omitted for brevity.

Prescribed boundary conditions at the upper and lower edges of the side-wall (herein a free condition) enable the unknowns in these equations (A_1, B_1, A_2, B_2) to be determined. The wave mobility of an infinite side-wall, $Y_\infty^s(k) = V(k)/F_y(k)$, can then be obtained by assuming $F_y(k) = h\sigma_y(k)$.

Based upon the infinite case, the mobility of a finite side-wall can be obtained via the method of images [3]. With this technique, a series of secondary forces are applied to the infinite side-wall in such a manner as to impose displacement conditions equivalent to a finite edge [4, 5]. For a zero vertical displacement condition, forces of equal magnitude but of opposite direction have to be applied at image positions, whereas to satisfy a zero horizontal displacement condition the forces need to be of equal magnitude and in the same direction. These two conditions represent a roller and a guided edge respectively, (see Figure 1). Since a limitation of the image source technique, employing real-valued sources, is that it cannot represent a free boundary (necessitating that both the shear and normal stresses vanish at the edge), a roller condition is assigned to the edges of the side-wall. Whilst strictly speaking, a free rather than a guided condition would be most applicable for the side-wall, it is argued that, with respect to a test of the hypothesis, the use of either is valid since differences between the two conditions simply manifest themselves as subtleties in the eigenvalues of the side-wall.

For point excitation, the expression for the mobility of the finite side-wall is

$$Y^s(k) = \frac{i}{l_x} \sum_{m=0}^{\infty} \cos(m\Delta kx_0) Y_\infty^x(m\Delta k) \cos(m\Delta kx), \tag{18}$$
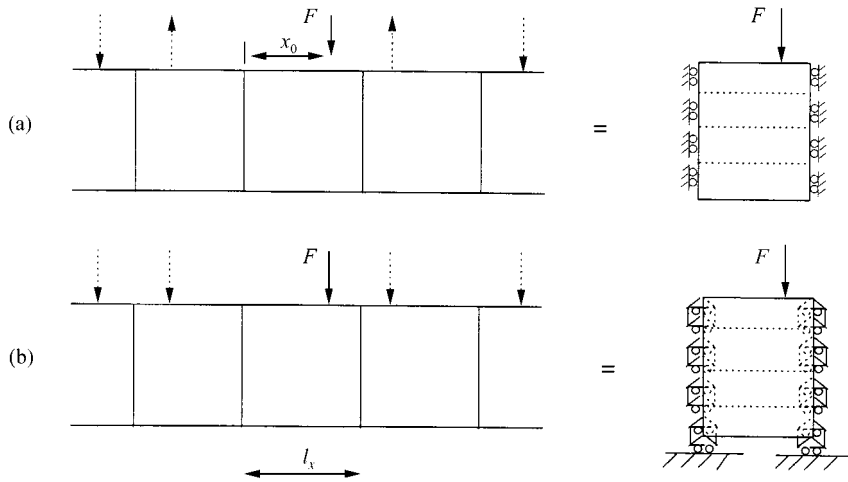
where $\Delta k = \pi/l_x$.

Figure 1. Image source distribution establishing (a) the guided and (b) the roller condition.

Without inflicting on the generality of the study, an infinite foundation plate can be considered appropriate for the recipient structure upon which the box is seated [6, 7]. Based upon thin plate theory the mobility of such a plate-like recipient is given in [3] as

$$Y_\infty^r = \frac{V(x, z)}{F(x_0, z_0)} = \frac{\omega 12(1 - v^2)}{8Eh^3 k_B^2} \left[H_0^{(2)}(k_B r) - H_0^{(2)}(-ik_B r) \right]. \tag{19}$$

Since both this mobility and that of the side-wall are defined for discrete positions, it is convenient to connect the side-wall of the recipient using a series of discrete connections in the model (see Figure 2). If the upper edge to the side-wall is also considered discretized, any force distribution can be applied by synthesizing it from a sequence of point forces and employing superposition theory (see again Figure 2).

Thence, connecting the side-wall and recipient plate using N points leads to the following matrix equation:

$$\begin{bmatrix} (Y_s^{L11} + Y_r^{L11}) & (Y_s^{L21} + Y_r^{L21}) & \cdots & (Y_s^{LN1} + Y_r^{LN1}) \\ (Y_s^{L12} + Y_r^{L12}) & (Y_s^{L22} + Y_r^{L22}) & \cdots & (Y_s^{LN2} + Y_r^{LN2}) \\ \cdots & \cdots & \cdots & \cdots \\ (Y_s^{L1N} + Y_r^{L1N}) & (Y_s^{L2N} + Y_r^{L2N}) & \cdots & (Y_s^{LNN} + Y_r^{LNN}) \end{bmatrix} \begin{bmatrix} F_s^{L1} \\ F_s^{L2} \\ \cdots \\ F_s^{LN} \end{bmatrix} = \begin{bmatrix} -Y_s^{UL11} \\ -Y_s^{UL21} \\ \cdots \\ -Y_s^{ULN1} \end{bmatrix} \begin{bmatrix} F_s^{U1} \\ F_s^{U2} \\ \cdots \\ F_s^{UN} \end{bmatrix}. \tag{20}$$

From the Nyquist criterion, a reliable solution for $k_B l_x < 10\pi$ can be obtained for a discretization involving more than 10 contact points.

Upon solving equation (20) for the forces at the side-wall/recipient interface, the velocities along the upper edge of the side-wall can be obtained from

$$V^{Um} = \sum_{n=1}^{N} Y_s^{Umn} F_s^{Un} + Y_s^{ULmn} F_s^{Ln}, \tag{21}$$
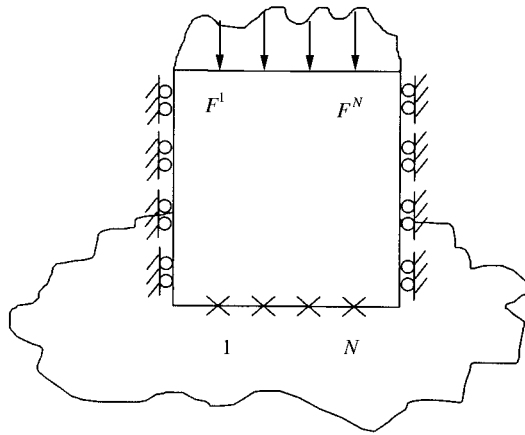
Figure 2. Discretisations of the line connection and force distribution.

and subsequently the total input power is determined from

$$W_{top} = \tfrac{1}{2}\mathrm{Re}\left\{ \sum_{n=1}^{N} V^{Un}F^{Un*} \right\}. \tag{22}$$

For a square faced side-wall, attached to a thick recipient plate, the power is shown in Figure 3 for two different cases of force excitation: W_{point} is for a point force positioned at the mid-position of the side-walls upper edge and $W_{uniform}$ is for a force distributed uniformly along this edge. For both cases, the normalization is with respect to the power that would be manifested if the recipient plate was to be excited directly by the point force; i.e. $W^{\infty} = |F|^2/16(Eh_{rec}^4\rho/(12(1-v^2)))^{1/2}$ [3].

As can be expected, the lower asymptote is comparable for both cases and is the power input to the directly excited recipient plate. For $W_{uniform}$ the upper asymptote is that for an equivalent infinite rod, $W_{rod} = |F|^2/2S\sqrt{E\rho}$, whilst for W_{point} the trend for high Helmholtz numbers is approximately a decade below this [5]. Marked differences between the two cases are observed in the resonant region for $W_{uniform}$ only mimics W_{point} at certain resonances. The simple explanation for this is that a uniform force distribution can only excite longitudinal waves whilst a point force excites both longitudinal and transverse waves. With the current side-wall dimensions these transverse resonances are the second, fourth, etc., seen in the point force case (for other dimensions the "order" of these resonances will, of course, be different). Thus, for a clear physical reason, any resonances associated with strong transverse motion cannot be captured by using a uniform force distribution.[‡] This constitutes a limitation of the proposed hypothesis.

In practice, however, where the excitation will be at an interior position of the top-plate of the box, the forces established along the upper edges of the side-walls can be expected to be more spatially distributed than point-like. Since the spatially distributed case represents the situation from which the hypothesis was drawn it is argued that the above point force result represents the limiting and "worst-case" scenario. To provide a more representative distribution, a top-plate should therefore be "attached" to the side-wall and excited at an interior point.

[‡] The small 'responses' seen at these resonances for the uniform load are associated with the limited number of discretised points; if the number of points were infinite these would be suppressed completely.
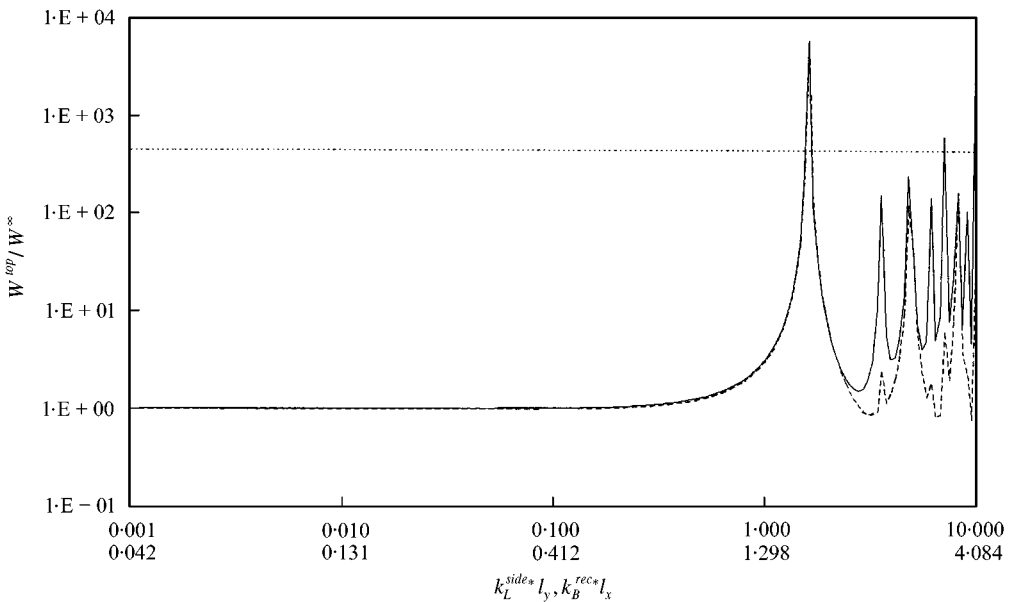
Figure 3. Total power for uniform and point excitation at upper edge of a square-shaped ($l_y/l_x = 1$) side-wall, $h_{side}/h_{rec} = 0.01$. —— W_{point}, – – – – $W_{uniform}$, - - - - W_{rod}.

One way to investigate the effect of a top-plate is to assume that it is simply supported at all edges[§] and supply the force distribution resultant along one edge to the upper edge of the side-wall (see Figure 4). With a point force "on" the top-plate at (x_0, z_0) the force distribution imposed upon the side-wall is then given by

$$F(x, 0) = \frac{F_0 h^3 E}{12(1 - v^2)\rho h l_x l_z}$$

$$\times \sum_{m=1}^{\infty} \sum_{n=1}^{\infty} \frac{\sin(m\pi x_0 l_x)\sin(n\pi z_0/l_z)}{\omega_{mn}^2(1 + i\eta) - \omega^2} \left(\frac{n\pi}{l_z}\right) \sin\left(\frac{m\pi x}{l_x}\right) \cos\left(\frac{n\pi z}{l_z}\right)$$

$$\times \left\{\left(\frac{n\pi}{l_z}\right)^2 + \left(\frac{m\pi}{l_x}\right)^2\right\}. \tag{23}$$

Assuming an aspect ratio of $1:2$ for the top-plate and the excitation force at a central position, the power transmitted at the upper edge of the side-wall, $W_{complete}$, is shown in Figure 5. Also shown are two estimates ($W_{uniform}(k)$ and $W_{uniform}$) based upon uniform force distributions. The difference between the two estimates is that for $W_{uniform}(k)$ the spatial average of the complete force distribution is calculated as a function of wavenumber k whilst for $W_{uniform}$ this spatial average is simply assigned the value obtained from the static case. $W_{uniform}$ is therefore invariant with wavenumber. As before, all results are normalized with respect to the power input to the point-excited recipient plate.

For low Helmholtz numbers the asymptotic trend is towards the normalization factor whilst for higher Helmholtz number a succession of resonances are displayed. Below

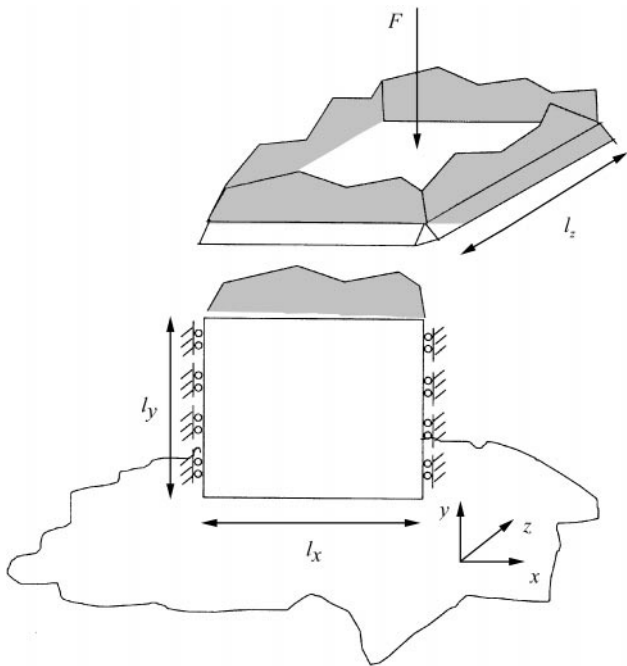[§] Such a condition approximates to that observed experimentally [8, 9].

Figure 4. A force distribution from a simply supported top-plate imposed onto a side-wall.
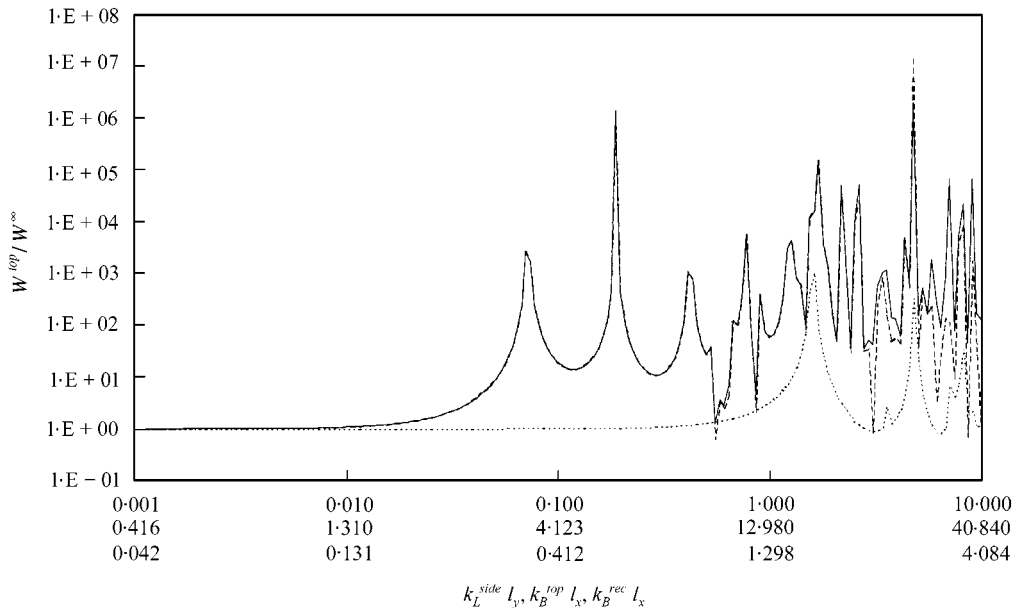

Figure 5. Total power for force at $(0.5\,l_x, 0.5\,l_z)$ on top plate, $l_z/l_x = 2$, $l_y/l_x = 1$, $h_{side}/h_{rec} = 0.01$, $h_{top}/h_{rec} = 0.01$. —— $W_{complete}$, – – – – $W_{uniform}(k)$, - - - - $W_{uniform}$.

$k_L^{side}l_y = \pi/2$ these resonances are only associated with the top-plate, whilst above, some are also associated with the side-wall. $W_{uniform}$ reveals which of these are allied with longitudinal waves. It is suggested that $W_{uniform}(k)$ is reliable for Helmholtz numbers $k_L^{side}l_y < 2\pi$. The limit coincides, approximately, with that wavenumber where the width of the side-wall
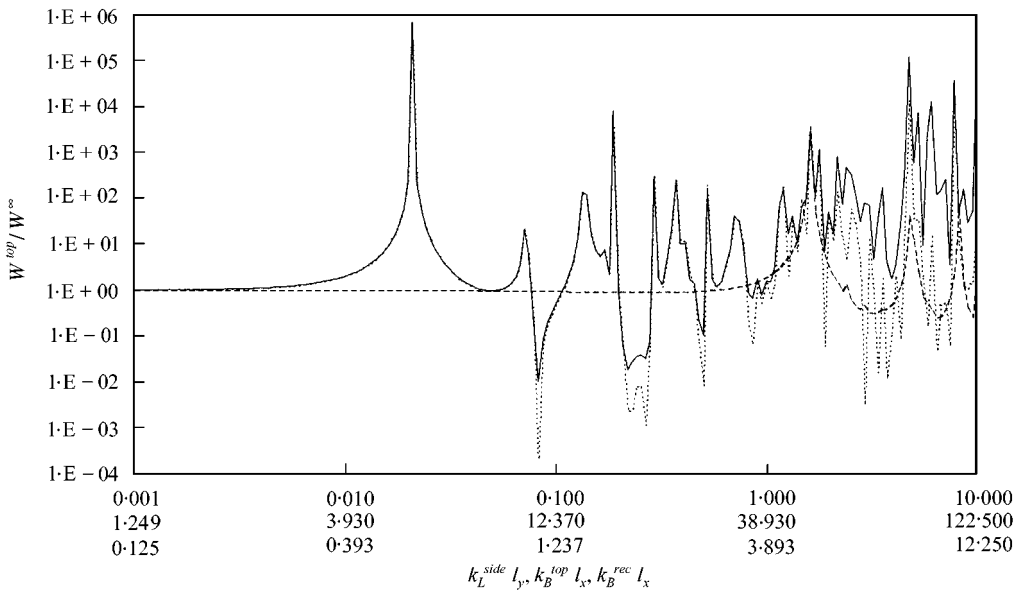
Figure 6. Total power for force at $(0.5\,l_x, 0.5\,l_z)$ on top plate, $l_z/l_x = 2$, $l_y/l_x = 1/3$, $h_{side}/h_{rec} = 0.01$, $h_{top}/h_{rec} = 0.01$. —— $W_{complete}$, – – – – $W_{uniform}(k)$, - - - - $W_{uniform}$.

equals the quasi-longitudinal wavelength; i.e., the resonance where the wave retraces itself in the "left/right" direction. Physically, this marks the transition from the force distribution being "quasi-static" to it being "wave-like". Thus, a criterion for the estimate to be reliable is when the longitudinal wavelength is less than the width of the side-wall. For an elongated side-wall where, for example, $l_x/l_y = 3$, the limit of reliability is therefore at a lower Helmholtz number and falls at $k_L^{side} l_y = 2\pi/3$ (see Figure 6).

With the square-faced side-wall, the "reliable" range was seen to include the first transverse resonance of the side-wall. This is of much interest, for it suggests that low order transverse waves are not excited significantly when the force along the upper edge of the side-wall is spatially distributed and "quasi-static". For this condition, it is clearly of interest to consider the excitation force at positions closer to the side-wall, whereby the closer the force to the edge the more "spatially concentrated" the force distribution, the limiting case being, of course, direct point excitation of the side-wall as in Figure 3. Hence, for the force at positions $(0.5\,l_x, 0.25\,l_z)$ and $(0.5\,l_x, 0.1\,l_z)$, Figures 7 and 8 are obtained.

Considering the maxima, both results again suggest that the approximate solution $W_{uniform}(k)$ is reliable for Helmholtz numbers up to that wavenumber where the width of the side-wall equals the quasi-longitudinal wavelength; i.e., even at the 'troublesome' transverse resonance of the side-wall $W_{uniform}(k)$ is within a decade of $W_{complete}$. Although the discrepancies are greater at the minima it can be argued that for engineering practice this is of limited consequence, the argument being, that the primary aims of such analyses are establishing the dominant resonances and estimating the power transmission. From the two Figures the significant observation is, therefore, that the reliability of $W_{uniform}(k)$ appears to be "insensitive" to the proximity of the input force relative to the edge of the side-wall. Although in this respect Figure 8 is encouraging, some caution should, of course, be exercised with this statement in view of Figure 3.

In order to study the influence of the loss factor, Figure 9 is presented. The result can be compared with Figure 5 since both are obtained for the same system but with different loss
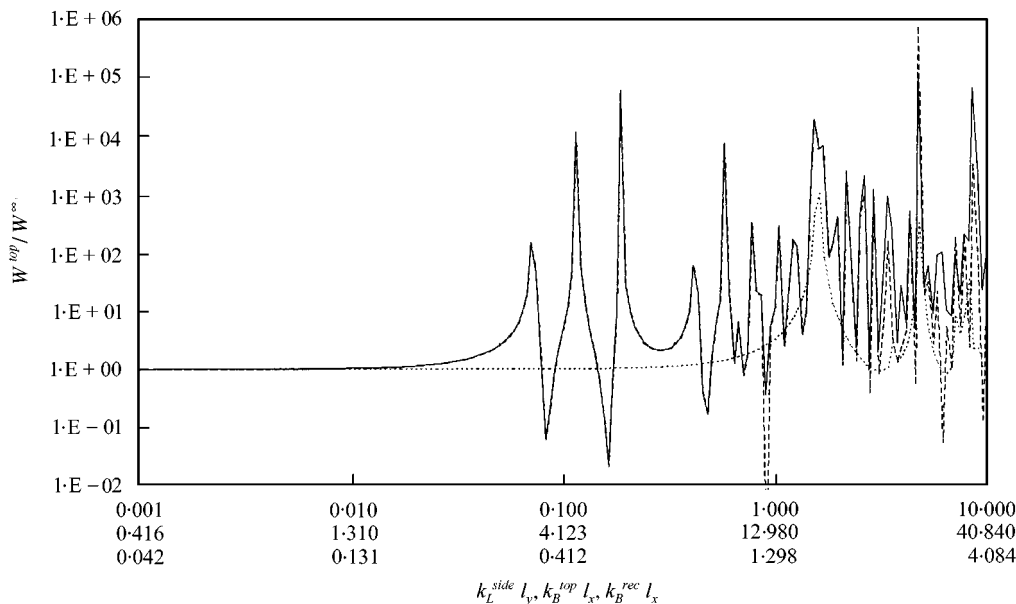
Figure 7. Total power for force at $(0.5\,l_x, 0.25\,l_z)$ on top plate, $l_z/l_x = 2$, $l_y/l_x = 1$, $h_{side}/h_{rec} = 0.01$, $h_{top}/h_{rec} = 0.01$. —— $W_{complete}$, ---- $W_{uniform}(k)$, ---- $W_{uniform}$.

Figure 8. Total power for force at $(0.5\,l_x, 0.1\,l_z)$ on top plate, $l_z/l_x = 2$, $l_y/l_x = 1$, $h_{side}/h_{rec} = 0.01$, $h_{top}/h_{rec} = 0.01$. —— $W_{complete}$, ---- $W_{uniform}(k)$, ---- $W_{uniform}$.
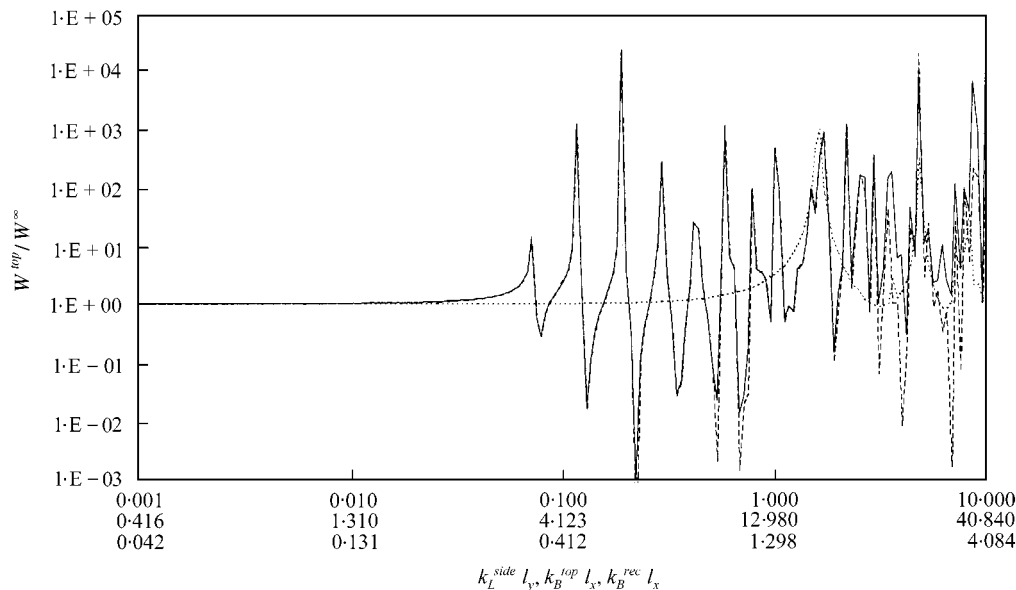
factors: a value of 0·0001 for Figure 5 and a value of 0·01 for Figure 9. Whilst in Figure 9 the resonance peaks are, as can be expected, smaller, $W_{uniform}(k)$ remains reliable up to that wavenumber where the width of the side-wall equals the quasi-longitudinal wavelength. It is indicated therefore that the accuracy of $W_{uniform}(k)$ is insensitive to the loss factor.
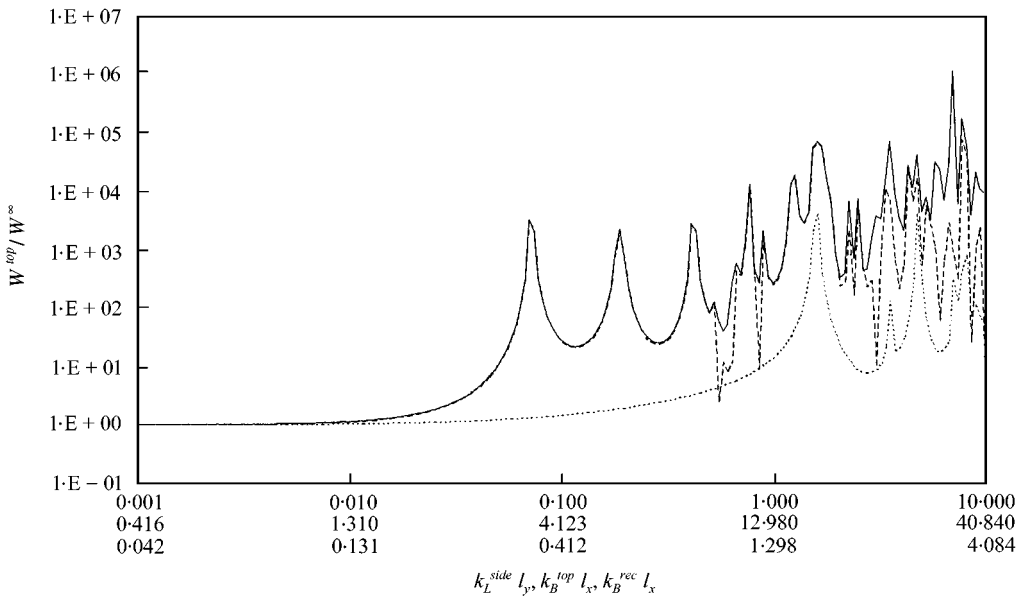
Figure 9. Total power for force at $(0.5\,l_x, 0.5\,l_z)$ on top plate, $l_z/l_x = 2$, $l_y/l_x = 1$, $h_{side}/h_{rec} = 0.01$, $h_{top}/h_{rec} = 0.01$. $h = 0.01$. —— $W_{complete}$, – – – $W_{uniform}(k)$, - - - - $W_{uniform}$.

3. POWER TRANSMISSION FOR A BOX

In a similar manner, a complete box can be constructed by connecting four side-walls to the recipient plate and imposing a force distribution upon the upper edge of each side-wall under the assumption that the distribution is that of a simply supported top-plate (see Figure 10). The fact that a force distribution on the upper edge of the side-walls is applied directly means that the model does not have to include structural coupling between these edges via the top-plate. Also, since a roller condition is imposed at the vertical edges of the side-walls, there is no transfer of vibrational power across these (vertical) boundaries either. However, coupling between the side-walls via the recipient plate is present.

With reference to Figure 11 the matrix equation to be solved for the forces along the box/recipient interface is

$$
\begin{bmatrix}
[Y^L_{sr11}] & [Y^L_{r21}] & [Y^L_{r31}] & [Y^L_{r41}] \\
[Y^L_{r12}] & [Y^L_{sr22}] & [Y^L_{r32}] & [Y^L_{r42}] \\
[Y^L_{r13}] & [Y^L_{r23}] & [Y^L_{sr33}] & [Y^L_{r43}] \\
[Y^L_{r14}] & [Y^L_{r24}] & [Y^L_{r34}] & [Y^L_{sr44}]
\end{bmatrix}
\cdot
\begin{bmatrix}
[F^L_{11}] \\
[F^L_{22}] \\
[F^L_{33}] \\
[F^L_{44}]
\end{bmatrix}
$$

$$
=
\begin{bmatrix}
[Y^{UL}_{s11}] & [0] & [0] & [0] \\
[0] & [Y^{UL}_{s22}] & [0] & [0] \\
[0] & [0] & [Y^{UL}_{s33}] & [0] \\
[0] & [0] & [0] & [Y^{UL}_{s44}]
\end{bmatrix}
\cdot
\begin{bmatrix}
[F^U_{11}] \\
[F^U_{22}] \\
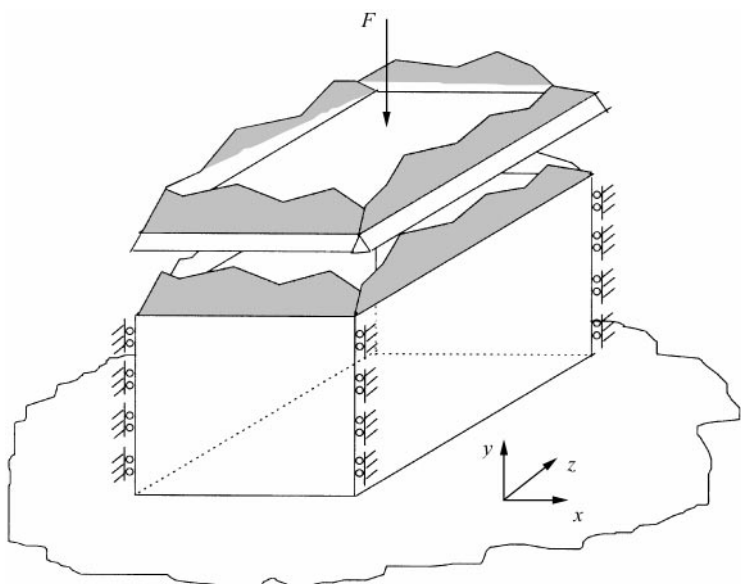[F^U_{33}] \\
[F^U_{44}]
\end{bmatrix},
\tag{24}
$$

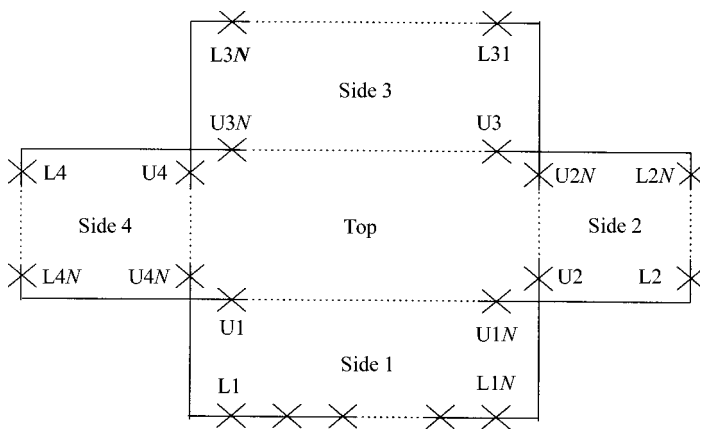Figure 10. The box attached to an infinite plate recipient.

Figure 11. Discretization of edge connections along the box (shown folded out).

where $[\mathbf{Y}^L_{sr_{mm}}]$ is a sub-matrix designating the summation of the side-wall and recipient mobilities at the lower edge of side-wall m. It is given by

$$[\mathbf{Y}^L_{sr_{mm}}] = \begin{bmatrix} (Y^{L11}_{s_{mm}} + Y^{L11}_{r_{mm}}) & (Y^{L21}_{s_{mm}} + Y^{L21}_{r_{mm}}) & \cdots & (Y^{LN1}_{s_{mm}} + Y^{LN1}_{r_{mm}}) \\ (Y^{L12}_{s_{mm}} + Y^{L12}_{r_{mm}}) & (Y^{L22}_{s_{mm}} + Y^{L22}_{r_{mm}}) & \cdots & (Y^{LN2}_{s_{mm}} + Y^{LN2}_{r_{mm}}) \\ \cdots & \cdots & \cdots & \cdots \\ (Y^{L1N}_{s_{mm}} + Y^{L1N}_{r_{mm}}) & (Y^{L2N}_{s_{mm}} + Y^{L2N}_{r_{mm}}) & \cdots & (Y^{LNN}_{s_{mm}} + Y^{LNN}_{r_{mm}}) \end{bmatrix}, \qquad (25)$$

where N is the number of points in the discretization along each edge.

Similarly, $[\mathbf{Y}^L_{r_{mm}}]$ is a sub-matrix describing the transfer mobilities of the recipient between the lower edges of side-walls m and n. $[\mathbf{Y}^{UL}_{s_{mm}}]$ constitutes the transfer between the upper and the lower edges of side-wall m. $[\mathbf{F}^U_{mm}]$ and $[\mathbf{F}^L_{mm}]$ define the forces at the upper and lower edges respectively of side-wall m with $[\mathbf{F}^U_{mm}]$ derived from equation (23).

The dimension of the system of equations is $(4N, 4N)$ and to satisfy the Nyquist criterion for $k_B l_x < 10\pi$, equation (24) will involve the accumulation of 1600 mobilities and then, formally, an inversion of a 40×40 matrix. Although by using reciprocity and symmetry the number of individual mobilities can be reduced to 400 the mechanics of the calculation remain considerable and highlights the real need to develop a simplified model.

The first box considered is configured with a top-plate of aspect ratio $1:2$, facing side-walls of aspect ratio $1:1$ and a thick recipient plate. With point excitation at the mid-position of the top-plate the complete transmitted power through the upper edge is shown in Figure 12, along with the $W_{uniform}(k)$ and $W_{uniform}$ estimates. Except for a large discrepancy just below the first transverse mode, $W_{uniform}(k)$ is found to describe reliably the transmission for Helmholtz numbers up to that wavenumber where the width of the longest side-wall equals the quasi-longitudinal wavelength, i.e., $k_L^{side} l_y = \pi$. The applicable range is therefore similar to that seen for a single side-wall.

For a box of more extreme dimension, $l_x/l_y = 1$, $l_z/l_x = 5$, corresponding results are shown in Figure 13. The suggestion again is that $W_{uniform}(k)$ is reliable for Helmholtz numbers below that wavenumber where the width of the longest side-wall equals the quasi-longitudinal wavelength, i.e., $k_L^{side} l_y = 2\pi/5$.

In Figure 14 results are shown for a box (of dimension $l_x/l_y = 1$, $l_z/l_x = 2$) excited at an off-centre position $(0\cdot4\,l_x, 0\cdot4\,l_z)$. Again, $W_{uniform}(k)$ is observed to provide reliable results up to that wavenumber where the width of the longest side-wall equals the quasi-longitudinal wavelength.
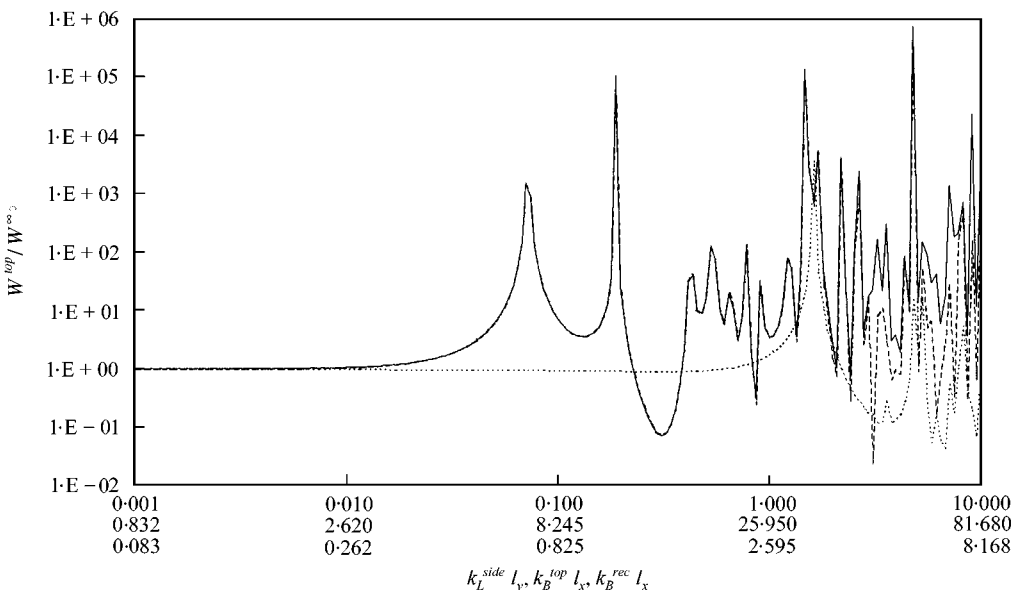

Figure 12. Total power for box, force at $(0\cdot5\,l_x, 0\cdot5\,l_z)$ on top plate, $l_z/l_x = 2$, $l_y/l_x = 1$, $h_{side}/h_{rec} = 0\cdot01$, $h_{top}/h_{rec} = 0\cdot01$. —— $W_{complete}$, – – – – $W_{uniform}(k)$, · · · · $W_{uniform}$.

Figure 13. Total power for box, force at $(0.5\,l_x, 0.5\,l_z)$ on top plate, $l_z/l_x = 5$, $l_y/l_x = 1$, $h_{side}/h_{rec} = 0.01$, $h_{top}/h_{rec} = 0.01$. —— $W_{complete}$, – – – – $W_{uniform}(k)$, - - - - $W_{uniform}$.
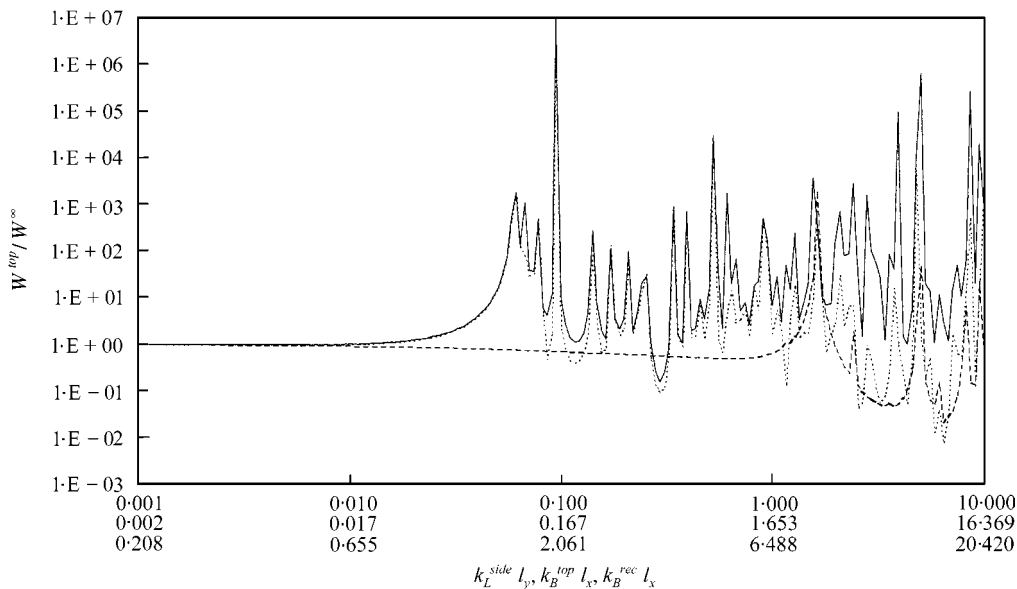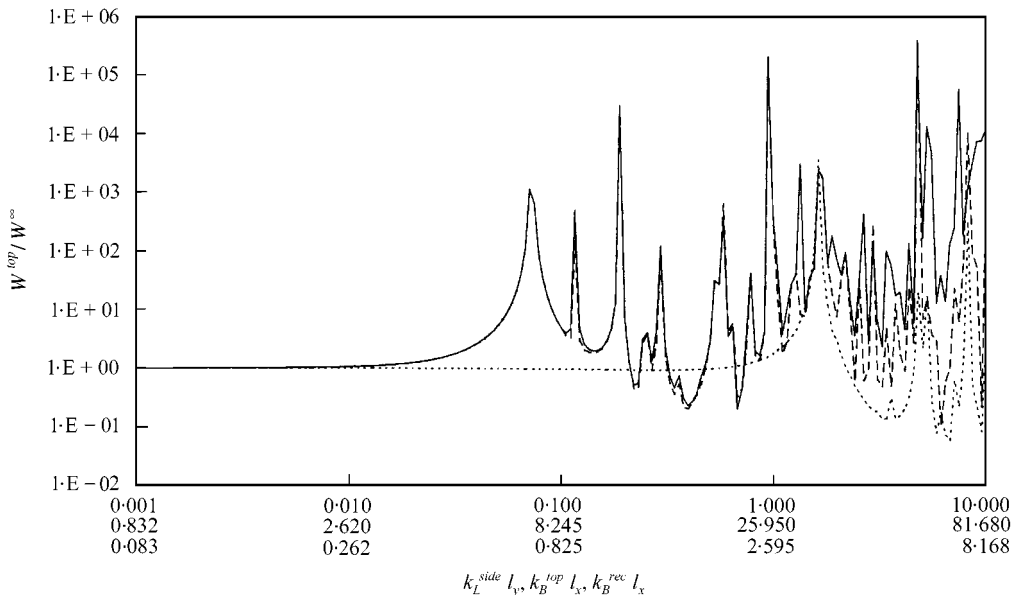

Figure 14. Total power for box, force at $(0.4\,l_x, 0.4\,l_z)$ on top plate, $l_z/l_x = 2$, $l_y/l_x = 1$, $h_{side}/h_{rec} = 0.01$, $h_{top}/h_{rec} = 0.01$. —— $W_{complete}$, – – – – $W_{uniform}(k)$, - - - - $W_{uniform}$.

3.1. SOLUTION USING EFFECTIVE STRIP MOBILITIES

For all the above models the approximate results have been based upon reducing the "true" force distribution along the upper edge(s) of the side-wall(s) to a uniform distribution. A further step to take is, of course, also to reduce the force distribution along

the lower edge(s) of the side-wall(s) to a uniform one. One significance of this advance is that it permits the box to be modelled via an effective strip mobility formulation [9, 10] where, in essence, an effective strip mobility is (in a spatial context) an "overall" mobility. It is realized by assuming a distribution for the force. For the box, the effective strip mobilities, Y^Σ, are defined as

$$Y_{sr_{mm}}^{\Sigma UL} = \int_0^{l_{x,z}} \int_0^{l_{x,z}} Y_{s,r_{mm}}^{U,L}(x, z_1 | x, z_2) \partial x, z_1 \, \partial x, z_2,$$
(26)

where $Y_{s,r_{mm}}^{U,L}(x, z_1 | x, z_2)$ is the mobility at either the upper or lower edge of side-wall m in direction x or z as appropriate and where the assumed force distribution is uniform.

A consequence of its definition is that the effective strip mobility is analogous to the point mobility. In a formulation based upon this, each edge of the side-walls the box can therefore be considered to be connected to the top-plate and the recipient plate at single "points". A solution to the box is thus forthcoming upon solving only for four unknown forces—one for each of the lower edges of the side-walls; that is

$$\begin{bmatrix} (Y_{s11}^{\Sigma L} + Y_{r11}^{\Sigma L}) & Y_{r21}^{\Sigma L} & Y_{r31}^{\Sigma L} & Y_{r41}^{\Sigma L} \\ Y_{r12}^{\Sigma L} & (Y_{s22}^{\Sigma L} + Y_{r22}^{\Sigma L}) & Y_{r32}^{\Sigma L} & Y_{r42}^{\Sigma L} \\ Y_{r13}^{\Sigma L} & Y_{r23}^{\Sigma L} & (Y_{s33}^{\Sigma L} + Y_{r33}^{\Sigma L}) & Y_{r43}^{\Sigma L} \\ Y_{r14}^{\Sigma L} & Y_{r24}^{\Sigma L} & Y_{r34}^{\Sigma L} & (Y_{s44}^{\Sigma L} + Y_{r44}^{\Sigma L}) \end{bmatrix} \cdot \begin{bmatrix} F_{11}^L \\ F_{22}^L \\ F_{33}^L \\ F_{44}^L \end{bmatrix} = \begin{bmatrix} Y_{s11}^{\Sigma UL} F_{11}^U \\ Y_{s22}^{\Sigma UL} F_{22}^U \\ Y_{s33}^{\Sigma UL} F_{33}^U \\ Y_{s44}^{\Sigma UL} F_{44}^U \end{bmatrix}.$$
(27)

Though closed-form expressions for many of the effective strip mobilities involved are given in Appendix A, expressions are missing for the effective strip transfer mobilities of the recipient plate. For these, the troublesome integrals can, however, be computed using a straightforward numerical routine.

In order to assess the implications of employing uniform force distributions throughout, Figure 15 is shown which can be compared with Figure 12 since both arise from the same configuration of box. Any differences between $W_{effective}$ and $W_{uniform}(k)$ are thus seen to be negligible. This suggests therefore that for a wide range of Helmholtz numbers, a reliable estimate of the power can be obtained assuming a uniform force distribution at both the upper and lower edges of the side-walls.

4. CONCLUDING REMARKS

The power transmitted first for a finite side-wall and then for a box-like structure connected to an infinite recipient plate has been studied. The side-wall(s) were assumed to carry in-plane motion only and to have a roller condition along their vertical edges.

A realistic distributed force was applied to the upper edge of the side-wall(s) and the forthcoming complete solution was compared with approximate solutions. The approximate solutions were obtained by imposing uniform force distribution(s) firstly along the upper edge of the side-wall(s) and then also along the lower edge.

When the spatial average of the exciting distributed force is known as a function of wavenumber, the forthcoming approximate solution is reproducing the power transmission reliably for all wavenumber up to that wavenumber where the width of the longest side-wall equals the quasi-longitudinal wavelength. A proviso, however, is that the excitation of the
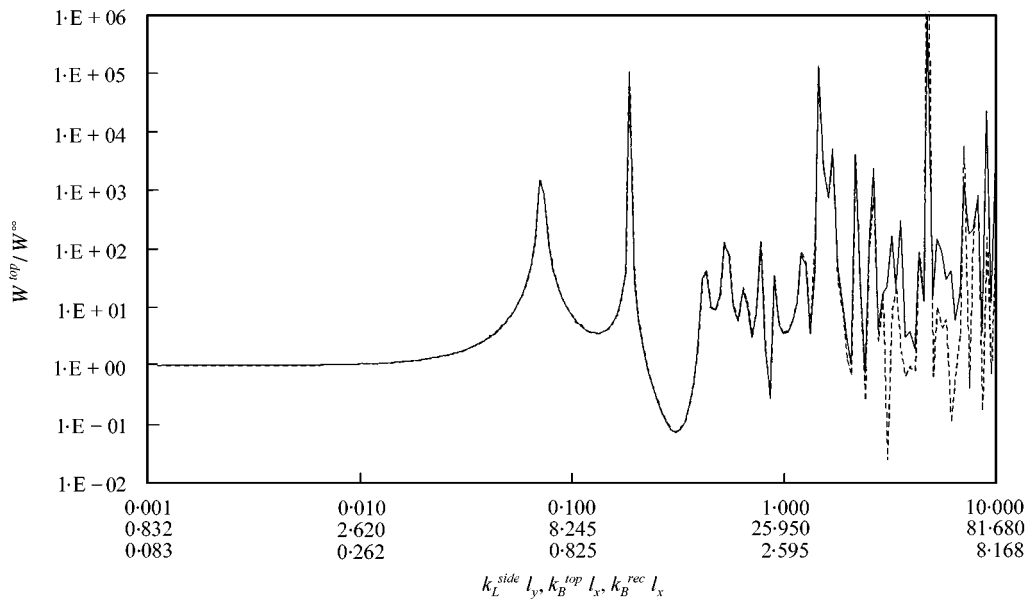
Figure 15. Total power for box using effective strip mobilities, force at $(0.5\,l_x, 0.5\,l_z)$ on top plate, $l_z/l_x = 2$, $l_y/l_x = 1$, $h_{side}/h_{rec} = 0.01$, $h_{top}/h_{rec} = 0.01$. —— $W_{complete}$, - - - - $W_{effective}$.

top-plate is such that the resulting exciting force distribution has a significant uniform component. This means that excitation positions close to the edges or corners of the top-plate can be handled but not positions actually at the edges. Discrepancies associated with shear resonances can, for example, be expected where the exciting force "distribution" is a point force applied directly to the upper edge of the side-wall.

When it is assumed that the force distribution along the lower edge is also uniform, an effective strip mobility formulation can be assumed in the same range. This reduces the mathematical description of the box to a simple set of linear equations involving only four unknown forces; one force per lower edge. If closed-form expressions for all the effective strip mobilities can be obtained this will therefore lead to simplified procedures for estimating the power transmission in box-like systems for wavenumbers below that wavenumber where the width of the longest side-wall equals the quasi-longitudinal wavelength.

In Part II of this two series paper, further simplifications applicable to the estimation of vibrational power in built-up structures are to be presented. These simplifications include the introduction of an infinite top-plate and the possibilities of reducing the "box" to a "can" with circular geometry. Final comparisons with experimental data will be shown.

REFERENCES

1. R. A. FULFORD and B. A. T. PETERSSON 1999 *Journal of Sound and Vibration* **227**, 479–510. The role of moments on the vibration transmission in built-up structures, Submitted.

2. B. A. T. PETERSSON 1992 *TNO Institute of Applied Physics*, *TPD-HAG-RPT*-92-227. Point mobilities of column seatings: theoretical basis and developments with respect to axial force excitation.
3. L. CREMER, M. HECKL and E. UNGAR 1973 *Structure-Borne Sound*. Berlin: Springer-Verlag, (second edition).
4. R. GUNDA, S. M. VIJAYAKER and R. SINGH 1995 *Journal of Sound and Vibration* **185**, 791–808. Method of images for the harmonic response of beams and rectangular plates.
5. S. H. LIU 1996 *Ph.D. Thesis, University of Southampton*. In-plane and flexural vibration in built-up plate structures.
6. E. NIJMAN, B. A. T. PETERSSON and F. VAN KNAAP 1992 *TPD-HAG-RPT*-92-201. *TNO Institute of Applied Physics, Department of Ship Acoustics*. An experimental study of the dynamic characteristics of full-scale ship double bottom structures.
7. F. J. FAHY and M. E. WESTCOTT 1978 *Journal of Sound and Vibration* **57**, 101–129. Measurements of floor mobility at low frequencies in some buildings with long floor spans.
8. B.A.T. PETERSSON 1993 *TPD-HAG-RPT*-93-0157, *TNO Institute of Applied Physics*. Preliminaries for pure transfer mobilities: beam- and frame-like structures.
9. B. A. T. PETERSSON and J. PLUNT 1980 *Report 80–19, Department of Building Acoustics, Chalmers University of Technology, Sweden*. Structure-borne sound transmission from machinery to foundations.
10. P. HAMMER and B. PETERSSON 1988 *Journal of Sound and Vibration* **129**, 119–132. Strip excitation; Part I: strip mobility.

APPENDIX A: EXPRESSIONS FOR THE EFFECTIVE STRIP MOBILITIES

For side-walls, closed-form expressions for the effective strip mobilities are given as

$$Y_{s11}^{\Sigma L} = Y_{s33}^{\Sigma L} = \frac{i\omega}{l_x k_L h(D + 2G)\sin(k_L l_y)}, \tag{A1}$$

$$Y_{s22}^{\Sigma L} = Y_{s44}^{\Sigma L} = \frac{i\omega}{l_z k_L h(D + 2G)\sin(k_L l_y)}, \tag{A2}$$

$$Y_{s11}^{\Sigma UL} = Y_{s33}^{\Sigma UL} = \frac{i\omega\cosh(k_L l_y)}{l_x k_L h(D + 2G)\sin(k_L l_y)}, \tag{A3}$$

$$Y_{s22}^{\Sigma UL} = Y_{s44}^{\Sigma UL} = \frac{i\omega\cosh(k_L l_y)}{l_z k_L h(D + 2G)\sin(k_L l_y)}. \tag{A4}$$

For the receiver plate, the effective point strip mobilities, obtained from reference [10], are

$$Y_{r11}^{\Sigma L} = Y_{r33}^{\Sigma L} = \frac{\omega}{8Bk_B^2} \sum_{M=0}^{\infty} \frac{(-1)^M}{(M!)^2} \left(\frac{k_B}{2}\right)^{2M} \frac{(x + l_x/2)^{2M+1}}{2M+1}$$

$$- \sum_{M=0}^{\infty} \frac{(-1)^M}{(M!)^2} \left(\frac{k_B}{2}\right) \frac{2M(x - l_x/2)^{2M+1}}{2M+1}, \tag{A5}$$

$$Y_{r11}^{\Sigma L} = Y_{r33}^{\Sigma L} = \frac{\omega}{8Bk_B^2} \sum_{M=0}^{\infty} \frac{(-1)^M}{(M!)^2} \left(\frac{k_B}{2}\right)^{2M} \frac{(x + l_z/2)^{2M+1}}{2M+1}$$

$$- \sum_{M=0}^{\infty} \frac{(-1)^M}{(M!)^2} \left(\frac{k_B}{2}\right)^{2M} \frac{2M(x - l_z/2)^{2M+1}}{2M+1}. \tag{A6}$$

Closed-form expressions for the effective strip transfer mobilities of the recipient are however difficult to develop due to the complicated function for the response position. However, these can instead be computed via a numerical integration routine based upon the following:

$$Y_{r12}^{\Sigma L} = Y_{r23}^{\Sigma L} = Y_{r34}^{\Sigma L} = \frac{\omega}{8Bk_B^2} \int_0^{l_x} \int_0^{l_z} [H_0^{(2)}(k_B r) - H_0^{(2)}(-ik_B r)] \, dz \, dx, \tag{A7}$$

where $r = \sqrt{(l_x - x)^2 + z^2}$,

$$Y_{r13}^{\Sigma L} = \frac{\omega}{8Bk_B^2} \int_0^{l_x} \int_0^{l_x} [H_0^{(2)}(k_B r) - H_0^{(2)}(-ik_B r)] \, dx_1 \, dx_2, \tag{A8}$$

where $r = \sqrt{(l_x - x_2 - x_1)^2 + l_z^2}$ and

$$Y_{r24}^{\Sigma L} = \frac{\omega}{8Bk_B^2} \int_0^{l_z} \int_0^{l_z} [H_0^{(2)}(k_B r) - H_0^{(2)}(-ik_B r)] \, dz_1 \, dz_2, \tag{A9}$$

where $r = \sqrt{(l_z - z_2 - z_1)^2 + l_x^2}$.

APPENDIX B: NOMENCLATURE

B	bending stiffness
C	wavespeed
D	modulus of elasticity
E	Young's modulus
F	force
G	modulus of rigidity
H	Hankel function
L	length
Q	complex power
S	area
V	velocity in the y direction
W	transmitted power
Y	mobility
f	component of force
h	thickness
i	imaginary unit
k	wavenumber
l	linear length

r	radical length
t	time
u	displacement in the x direction
v	displacement in the y direction
x, y, z	Cartesian co-ordinates
ϕ	dilatation
ψ	rotation
η	loss factor
v	Poisson's ratio
σ	normal stress
τ	shear stress
ω	angular frequency

Indices

B	bending wave
L	longitudinal wave
L	lower edge of side-wall
T	transverse wave
U	upper edge of side-wall
av	spatial average
r, rec	recipient plate
$s, side$	side-wall
top	top-plate
Σ	effective mobility
Φ	real part
Ψ	imaginary part

Notation

*	complex conjugate